Improvements and Complications Involved with Adding an 85-GHz Channel to Cloud Liquid Water Radiometers

Justin P. Bobak, *Member, IEEE,* and Christopher S. Ruf, *Senior Member, IEEE*

***Abstract*—The improvement in cloud-liquid estimates by a microwave radiometer with the addition of measurements at 85 GHz is quantified. Atmospheric emission is simulated from radiosonde data at frequencies commonly used by ground-based water-vapor radiometers (22.235 and 31.65 GHz) and also at 85.5 GHz. Retrieval algorithms are developed from opacities based on full Mie extinction by cloud droplets and under an assumption that ice effects are not significant for downwelling emission. The algorithms use either three frequencies or only the lower two. The inclusion of 85-GHz information significantly improves liquid-water path estimates at all levels of integrated liquid water. The Rayleigh approximation is shown to be valid for most cloudy conditions. Uncertainty in the calculated opacities due to varying cloud droplet-size distributions and liquid-water content profiles is quantified. The accuracy of a retrieval algorithm trained by Rayleigh approximation opacities and including the additional uncertainty is shown to provide estimates with error levels similar to those from the algorithm trained with full Mie opacities.**

***Index Terms*—Clouds, microwave measurement, radiometry.**

I. Introduction

MICROWAVE radiometry has been a tool for atmospheric research since the 1940's [1]. By the mid-1960's, the possibility of estimating the condensed cloud water integrated over an antenna-beam column was being discussed [2]. The techniques of cloud-liquid estimation by microwave radiometry are well documented [3]–[6]. Frequencies of 19.0 and 32.4 GHz for simultaneous estimation of integrated water vapor and integrated cloud liquid were suggested in [2]. While the choice of the lower frequency has been modified since that time [7], [8], the use of one (or two) channels on the water-vapor line centered at 22.235 GHz, and one channel in the atmospheric-transmission window near 31 GHz has become standard for ground-based water-vapor radiometers.

Liquid-water extinction increases monotonically with frequency in this portion of the microwave spectrum, so a frequency higher than 31 GHz, in conjunction with the standard frequencies, has potential for improving estimates of liquid-water path (LWP) [9]. Though higher frequency channels are common on satellite and airborne radiometers [10]–[12], their use in ground-based radiometers has been more limited [13]–[15]. This study has been undertaken in an attempt to quantify the benefits arising from the addition of a higher frequency channel to a ground-based radiometer and to examine some of the uncertainties arising from the modeling of cloud parameters. Modeling choices takes on greater importance at higher frequencies because of the relatively larger electrical size of the droplets.

In order to examine the effect of including higher frequency information in an LWP estimation algorithm, radiative-transfer calculations were made from radiosonde (RaOb) data. Since radiosondes cannot directly measure condensed liquid in clouds, a value was calculated based on assumptions that the liquid water in clouds behaved in a modified adiabatic fashion. A strictly adiabatic calculation of cloud-liquid water results in liquid-water contents that are greater than those actually observed in nature. This is due to the assumption (in adiabatic calculations) that air parcels are closed systems. This is inaccurate especially near the tops of clouds, where dry air is being entrained into the system [16]. However, the adiabatic approximation provides a good starting point. The adiabatic liquid-water content was calculated from RaOb-measured quantities [17]. This calculated value was then adjusted to provide a more realistic liquid-water profile. The details are presented in the Appendix. The integral over height of this calculated liquid-water content (LWC) was taken as the "true" LWP. Atmospheric opacities simulated from RaOb data were used to develop two LWP retrieval algorithms. The first algorithm includes two frequencies commonly used for LWP retrieval, 22.235 and 31.65 GHz. The second algorithm adds a third channel at 85.5 GHz. This latter retrieval provides a significantly improved fit to the true LWP, as calculated from RaOb data.

Several potential difficulties in the use of 85-GHz information are considered. Cloud-modeling choices assume increased importance as observation frequencies increase. Because the electrical size of cloud droplets increases with decreasing wavelength, the Rayleigh approximation for droplet extinction may no longer be valid, especially for clouds in which larger droplets are present in moderate numbers. Previous authors [14], [18] have ignored scattering by liquid droplets at 90 GHz, and the current work confirms that this is a valid assumption for clouds with integrated liquid of up to several hundred micrometers. However, the droplet-size distribution (DSD) (the statistical distribution of liquid in clouds as a function of droplet radius) has

Manuscript received February 3, 1998; revised November 10, 1998.

J. P. Bobak was with the Communications and Space Sciences Laboratory, The Pennsylvania State University, University Park, PA 16802 USA. He is now with the Remote Sensing Physics Branch, Naval Research Laboratory, Washington, D.C. 20375 USA.

C. S. Ruf is with the Communications and Space Sciences Laboratory, The Pennsylvania State University, University Park, PA 16802 USA (e-mail: ruf@kth.ee.psu.edu).

Publisher Item Identifier S 0196-2892(00)00009-7.

the potential to be significant at these frequencies. While multiple models for DSD exist in the literature [16], [19], [20], the actual DSD can vary widely from cloud type to cloud type, from cloud to cloud of the same type, and even from point to point within a single cloud [16], [21], [22].

Another cause for concern arises in choosing a form for the vertical distribution of liquid in a cloud, known as the LWC profile. Higher frequencies will suffer relatively greater attenuation over a given physical path length through a cloud due to droplet extinction, which as mentioned previously, increases monotonically in this portion of the spectrum. This deserves consideration when thicker clouds are present. In thick clouds, the temperature of the water, and thus its dielectric constant and extinction properties, can change significantly between the bottom and the top of the cloud. Unfortunately, the LWC profile is also quite variable [16].

Descriptions of pertinent cloud measurements and models are available in the literature [23]–[30]. Since neither the DSD nor the LWC profile may be assumed to follow any one model due to the variability in these quantities, they must be considered to be additional sources of uncertainty in the estimation of cloud liquid.

Section II discusses key points of the radiative-transfer calculation and includes an introduction to the different cloud models tested. Statistics of the RaOb data set are also presented. Section III describes the development of initial-retrieval algorithms and shows the improved retrieval accuracy that can be achieved through the addition of 85-GHz information. Section IV investigates the conditions under which the Rayleigh approximation can be used with confidence. In Section V, the uncertainty in calculated atmospheric opacity that arises from lack of knowledge of the appropriate DSD and LWC profile is quantified. Section VI shows the retrieval accuracy when the retrieval is trained with Rayleigh approximation opacities and includes the additional noise contributions from Section V. A summary and conclusions follow in Section VII.

II. Radiative-Transfer Calculations

Radiative transfer code developed at the Pennsylvania State University, University Park [31] was modified to include a variety of different DSD and LWC profile models. The code uses RaOb data to calculate atmospheric opacities and brightness temperatures for all possible combinations of these cloud parameters using both the Rayleigh approximation and the full Mie solutions. Clouds are assumed to be present at heights where the RaOb-measured relative humidity exceeded 94%. The dielectric constant of condensed water in the droplets was calculated according to [32], which provides equations for estimating the dielectric constant at a given water temperature. Multiple scattering and ground reflections are ignored, and clouds are assumed to be comprised of only water in liquid state (no ice).

The Rayleigh approximation, which neglects scattering, is commonly used for radiative-transfer calculations in water-vapor radiometer (WVR) retrieval algorithms [33]–[35]. The specific form of the DSD is inconsequential because Rayleigh extinction is only a function of the mass quantity of liquid water present and is independent of the size distribution of droplets. The LWC profile could, however, affect results. Droplet-size limits of the Rayleigh approximation for 85-GHz radiation has been discussed in [35].

The full Mie extinction is not commonly calculated in ground-based, water-vapor radiometry, because scattering effects are minimal at frequencies at which ground-based WVR's typically operate. Calculation of full Mie extinction is more computationally intensive than calculation of Rayleigh extinction and also requires the assumption of a DSD. As noted previously, droplet-size distribution is a difficult parameter to model, and it has potential importance at higher frequencies. Atmospheric emission was calculated using the full Mie solution for five different DSD models. Each has a unimodal, modified-Gamma distribution. The models include distributions with mode radii fixed at 5, 10, or 15 μm, one with linearly varying mode radii (5 μm at the bottom of the cloud to 15 μm at the top), and one with cloud type-dependent distribution-shape parameters [16], [19], [20], [36], [37]. The appendix contains more detailed information about these DSD models.

One way that this work departs from previous work is in the evaluation of calculations involving the DSD. No *a priori* limits were set on the maximum radius attainable by cloud droplets. For nonprecipitating clouds, 100 μm has been a commonly assumed upper limit for radii [38]. However, measurements of supercooled cloud drops with radii of several hundred micrometers have been reported [39], and quite often, rain is present within clouds, though no precipitation may be reaching the ground. It is important to include the effects of these large drops, which scatter radiation out of proportion to their small number concentrations. Therefore, for each cloud pixel, the cloud extinction [40]

$$\kappa_e \propto \int Q_s(r)p(r)\,dr \tag{1}$$

where κ_e (cloud extinction), Q_s (scattering cross-section), and p (droplet-size distribution) were integrated over increasing droplet radii r until it converged.

For both the Mie and the Rayleigh calculations, opacities and brightness temperatures were calculated based on three different LWC profile models. The LWC profile models included adiabatic liquid water multiplied by a factor that decreased vertically through the cloud, adiabatic liquid water multiplied by a constant factor, and constant liquid water throughout the cloud [22], [37], [41], [42]. See the Appendix for more details on these models.

The different combinations of the LWC profile models and DSD models result in fifteen different calculated emissions for Mie extinction, while the LWC profiles lead to three different emissions for Rayleigh extinction. Brightness temperatures were calculated at 22.235, 31.65, and 85.5 GHz. Earlier work had shown that 23.8 GHz quantities behaved similarly to those at 22.235 GHz for our purposes. Information at 50.4 GHz had been found to provide only minimal improvements in LWP estimation, probably because this frequency does not show the level of sensitivity to cloud droplets necessary for our purposes. The cloud-structure signatures that were sought are

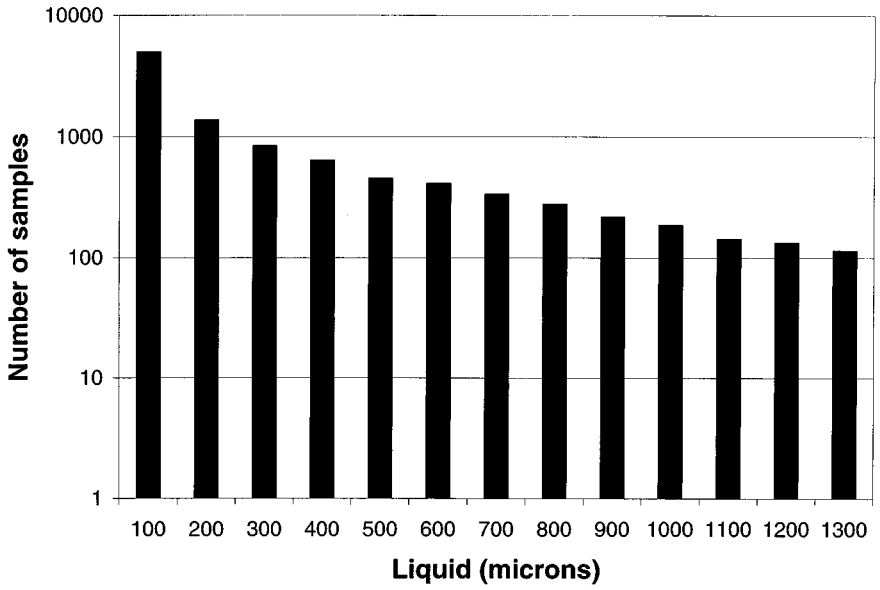

Fig. 1. Number of database radiosondes as a function of liquid-water path.

quite small in some cases. Since cloud extinction increases as the square of the frequency, signatures at a higher frequency are significantly more pronounced. The specific choice of 85.5 GHz was made to coincide with the SSM/I channel and because 90-GHz channels on upward-looking radiometers are currently of interest [14], [18]. The 90-GHz channels should behave similarly to the 85-GHz results presented here.

The RaOb data originated from 19 launch sites in the Western Pacific, Southern Atlantic, and Indian Oceans. All of the sites are located between -30° and $+30^\circ$ latitude. The radiosonde launch dates were from 1992 to 1997. RaOb's with integrated liquid amounts calculated to be from 1–2500 μm were used in the study. Approximately 10 300 RaOb's had LWP's in this range. For these RaOb's, the standard deviation of the calculated LWP's is 374 μm. The LWP distribution is shown in Fig. 1.

III. Motivation

In order to quantify the benefits of including 85 GHz information in a LWP retrieval algorithm, two algorithms were trained and tested on opacities resulting from what was considered to be the most realistic combination of DSD and LWC profiles (according to measurements as presented in the cloud literature). This combination was the exponentially decreasing fraction of adiabatic liquid water for the LWC profile model with the linearly varying mode radius DSD model.

Of approximately 10 300 RaOb's available, 500 were randomly chosen. Random noise with zero mean and the appropriate standard deviation as given in Table I was added to the opacity calculated at each frequency for each of these 500 RaOb's. This corresponds to uncertainty arising from the calculation of opacity based on a fixed value of effective radiating temperature and from radiometric precision (ΔT) of 0.1K. Increasing ΔT to 0.5K did not substantially change the error levels, so 0.1K was used in the rest of this work.

TABLE I
Uncertainty in Atmospheric Opacities Arising From Radiometric Precision of 0.1K and from Using a Constant Value for Effective Radiating Temperature

Frequency (GHz)	Standard deviation of added noise (Np)
22.235	0.0153
31.65	0.0176
85.5	0.0175

After the addition of noise, opacities from the 500 training RaOb's were used to calculate LWP retrieval coefficients through an MSE regression fit with LWP. Both a two-frequency and a three-frequency retrieval were developed. The resulting coefficients are

2 Frequency:

$$-352.1 - 1591\tau_{22} + 7123\tau_{32} = \mathrm{LWP}_1 \quad (2)$$

3 Frequency:

$$-88.45 - 1629\tau_{22} - 242.2\tau_{32} + 1347\tau_{85} = \mathrm{LWP}_1 \quad (3)$$

where LWP_1 is the estimated liquid-water path (micrometers), and τ_x is the opacity at frequency x (Nepers). A correction which was a function of the initial LWP estimate LWP_1 was added to remove a residual error in the estimates

2 Frequency:

$$\begin{aligned} 0 < \mathrm{LWP}_1 \le 100\,\mu\mathrm{m}; \quad \mathrm{LWP}_2 &= \mathrm{LWP}_1 - 17 \\ 100 < \mathrm{LWP}_1; \quad \mathrm{LWP}_2 &= 1.076\mathrm{LWP}_1 - 43 \end{aligned} \quad (2a)$$

3 Frequency:

$$\begin{aligned} 0 < \mathrm{LWP}_1 \le 100\,\mu\mathrm{m}; \quad \mathrm{LWP}_2 &= \mathrm{LWP}_1 - 11 \\ 100 < \mathrm{LWP}_1; \quad \mathrm{LWP}_2 &= 1.047\mathrm{LWP}_1 - 26 \end{aligned} \quad (3a)$$

where LWP_2 ia the corrected estimate of liquid-water path micrometers

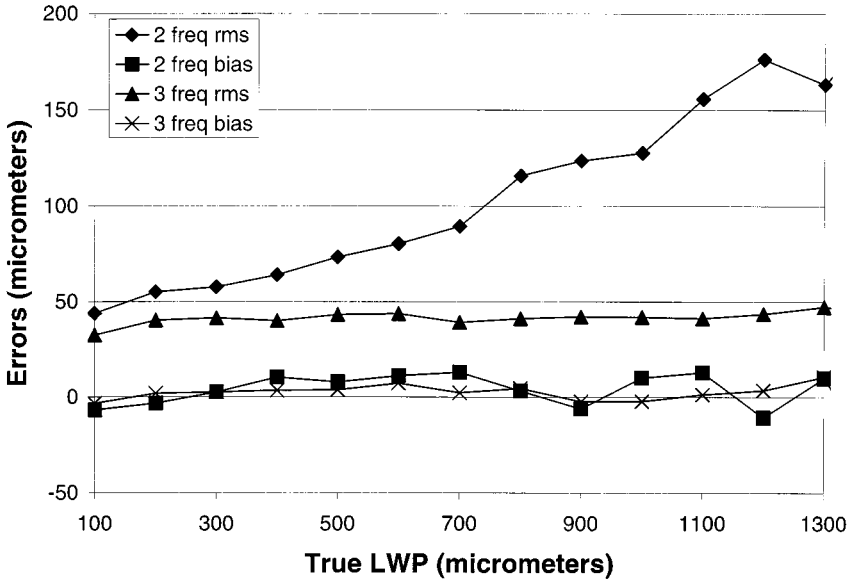

Fig. 2. Rms and bias errors as a function of liquid-water path for a two-frequency and a three-frequency retrieval, showing the improvement possible with the addition of 85-GHz information.

These retrievals were tested on the other approximately 9500 RaOb's. The resulting error statistics are

2 Frequency:

$$\text{rms error} = 85\,\mu\text{m}$$
$$\text{average bias} = 9\,\mu\text{m}$$

3 Frequency:

$$\text{rms error} = 41\,\mu\text{m}$$
$$\text{average bias} = 6\,\mu\text{m}.$$

The rms error and bias for each retrieval are shown in Fig. 2 as a function of LWP, where the results are cut off at 1300 μm due to small sample size above this level of LWP. Clearly, including information from the 85-GHz channel substantially improves the retrieval at all LWP levels. This increase in accuracy is particularly pronounced for large LWP, where the rms errors resulting from the three-frequency retrieval are one-fourth the size of those resulting from the two-frequency retrieval. Another positive result is the constant level of the three-frequency retrieval error with LWP. Large LWP's are retrieved with as much accuracy as small LWP's. The same is not true for the two-frequency retrieval.

The physical basis for the retrieval improvement is additional sensitivity of the 85-GHz channel to cloud liquid. The sensitivity of this channel is about five times greater than that of the 32-GHz channel [9] due to the relatively greater electrical size of cloud droplets at the higher frequency.

The benefits of including 85-GHz information are clear. However, these results were based on opacities calculated from the full Mie solution and with perfect knowledge of the DSD and LWC profiles. In the next section, the applicability of the Rayleigh approximation is investigated.

IV. Rayleigh Approximation

It is desirable to ascertain the conditions under which the Rayleigh approximation is valid. In order to do this, the difference between opacities calculated using the full Mie solution and those based on the Rayleigh approximation will be illustrated.

The question of LWC profile is not directly related to the Mie–Rayleigh question. Therefore, the response of calculated opacities to LWC profile was removed from consideration by comparing Mie opacities with Rayleigh opacities calculated using the same LWC profile model. In order to remove the effects of DSD uncertainty (which is also not of primary concern at this stage), only Mie opacities calculated from one model were used. The model chosen was the same as that used for Fig. 2.

The results are shown in Fig. 3. As expected, the 85-GHz opacities show the most departure from Rayleigh behavior. The error levels of the opacities (See Table I) are around 0.015 for each frequency. The worst errors occur at about 1000 μm integrated liquid for 85 GHz. Errors at the lower frequencies do not exceed this size, even for 2500 μm of integrated liquid (which would usually indicate rain). There is a small bias, since the Rayleigh opacities are almost always larger than the corresponding full Mie opacities, but this is small enough to be ignored under most circumstances.

For extremely thick clouds, the error induced by neglecting scattering at 85 GHz may become important. This situation will be discussed later, following a discussion of the uncertainty in opacities due to cloud parameters and a presentation of results of a retrieval for less extreme liquid-water paths using Rayleigh-calculated opacities.

V. Sensitivity of Emission to Cloud Models

There were a total of fifteen opacities calculated using the full Mie solution for each frequency and each RaOb in the data

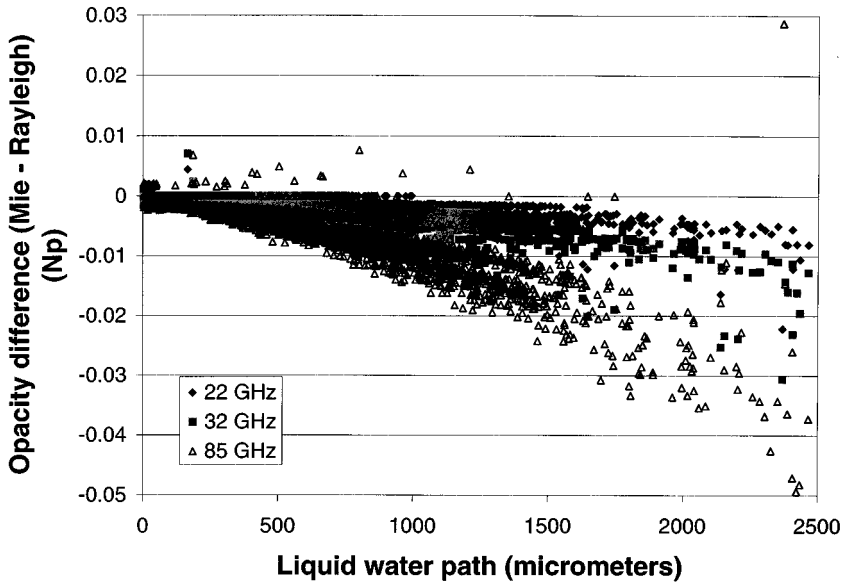

Fig. 3. Difference between opacities calculated using the full Mie solution and those calculated by using the Rayleigh approximation.

set. This corresponded to all possible combinations of five DSD models and three LWC profile models. The uncertainty due to each of these models will be dealt with separately. First, the sensitivity of opacity to DSD will be examined.

To remove effects from the LWC profile, only opacities calculated using the same model for the LWC profile were directly compared to one another. Then the maximum of the three values (corresponding to the three LWC profiles) was saved. The statistics calculated were the standard deviation of the five opacities and the difference between the maximum and the minimum of the five. The standard deviations are shown in Fig. 4. The maximum differences are shown in Fig. 5. Two branches are evident for each frequency. These correspond to the presence of one (or two) different cloud types and arise from the DSD model that was cloud-type dependent. The radiative-transfer code had a filter that loosely identified clouds as either stratus or fair-weather cumulus. Clouds were identified as stratus if a temperature inversion existed above the cloud, while most clouds not meeting the stratus definition were classified as fair-weather cumulus. The stratus clouds were responsible for the upper branch of each frequency in the figures, while the fair-weather cumulus lead to the lower branch. Compared to the noise levels in Table I, the standard deviation is significant at 85 GHz for LWP's of 500 μm or greater. For the two lower frequencies, the standard deviation is below the noise floor out to 2500 μm and beyond. As for the maximum differences between calculated opacities, this is still below the noise floor at all LWP for 22 GHz. However, at 32 GHz, it becomes significant around 1500 μm, and for 85 GHz, it is a cause for concern even at 200 μm.

The process for evaluating the effects of the uncertainty in the LWC profile was similar, but statistics were calculated over consistent DSD models, and the largest of the five resulting values (corresponding to five DSD's) were saved. The results are shown in Figs. 6 and 7. The uncertainty is insignificant for 22 and 32 GHz, but becomes important for LWP's of about 1000 μm or more when dealing with the 85-GHz opacities.

From these results, the effect of LWC profile model is relatively small and should not normally be a cause for concern. On the other hand, the DSD is a source of uncertainty that must be considered for all but the thinnest clouds when higher frequencies are used.

VI. Results for Operational Retrieval

In previous sections, we have shown that the Rayleigh approximation is valid for cloud-extinction calculations at 85 GHz, even for clouds that are quite thick. The uncertainty in calculated atmospheric opacities that results from a lack of knowledge regarding the DSD and LWC profile has also been shown. In this section, the results from a potential operational algorithm are presented. The retrieval was trained with opacities calculated using the Rayleigh approximation. The LWC profile used was the same as that used in the algorithm presented in Section III. The training opacities were modified by the addition of DSD and LWC profile uncertainty, in addition to the uncertainty arising from ΔT and lack of specific effective radiating-temperature information. The standard deviation of all 15 Mie solution opacities for each RaOb was calculated. Then the maximum values, corresponding to the assumed presence of only stratus clouds, were fit by a linear function of LWP to provide an estimate of opacity uncertainty that was a function of LWP. The relationships between the uncertainty in opacity and the LWP are as follows:

22 GHz:

$$\Delta\tau = 2.42 \times 10^{-6}\text{LWP} + 4 \times 10^{-6} \tag{4a}$$

32 GHz:

$$\Delta\tau = 4.76 \times 10^{-6}\text{LWP} - 3 \times 10^{-5} \tag{4b}$$

85 GHz:

$$\Delta\tau = 2.80 \times 10^{-5}\text{LWP} - 4 \times 10^{-5} \tag{4c}$$

where $\Delta\tau$ is the uncertainty in opacity due to cloud modeling (Np).

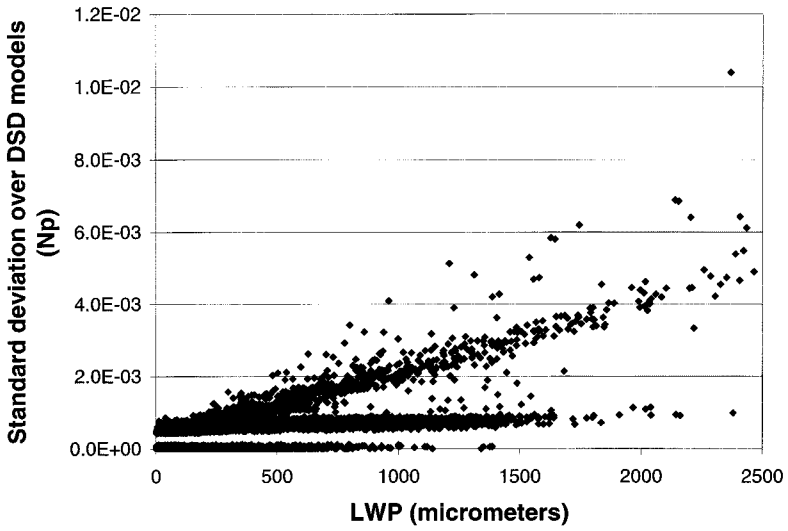

(a)

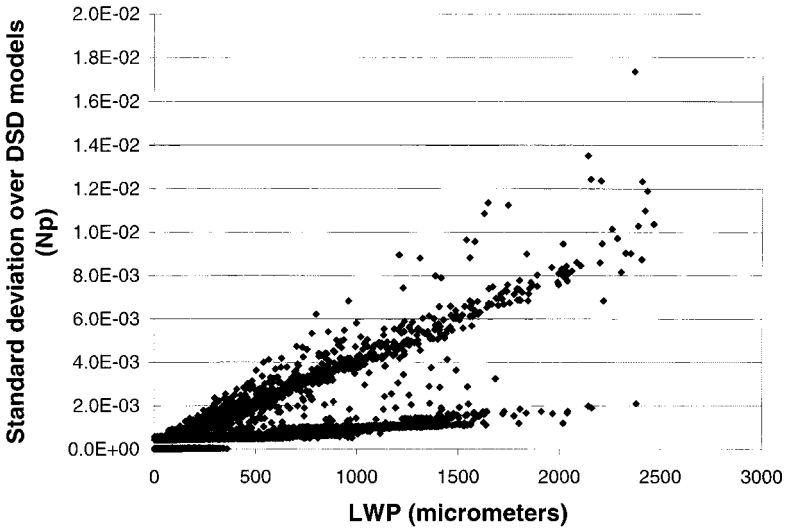

(b)

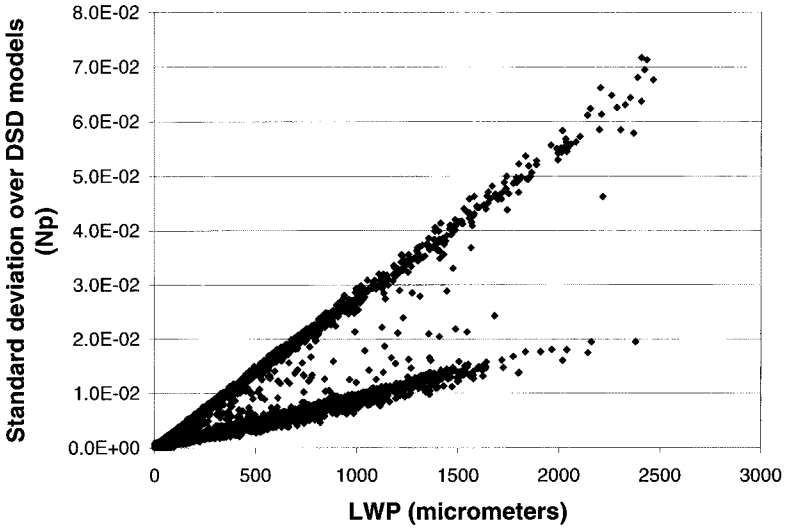

(c)

Fig. 4. Standard deviation of full Mie solution opacities over five DSD models. The points in the graphs are the maximum values out of three calculated standard deviations for each RaOb, corresponding to three different LWC profile models: (a) 22 GHz, (b) 32 GHz, and (c) 85 GHz.

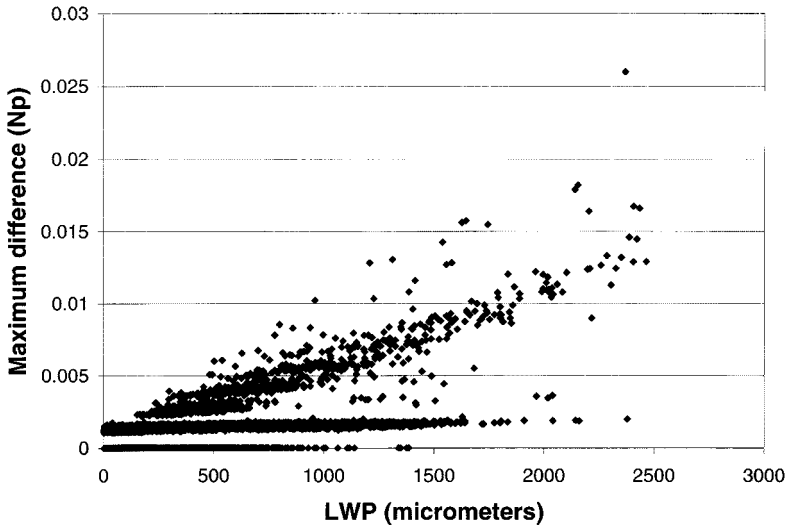

(a)

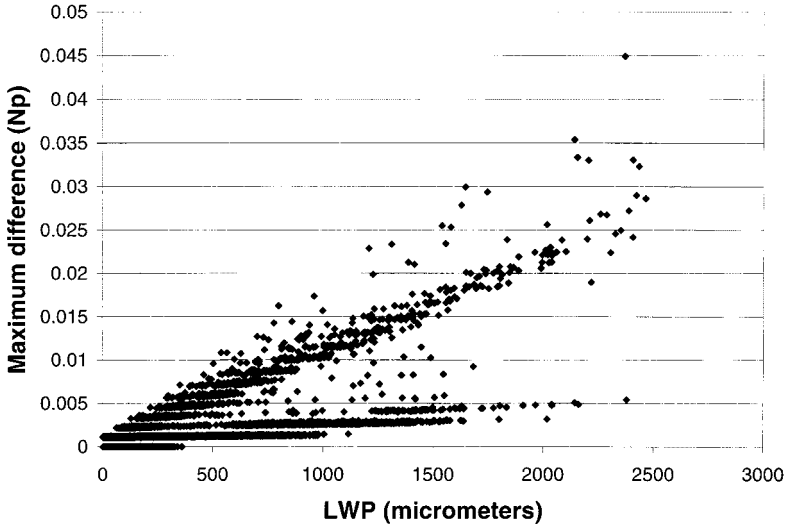

(b)

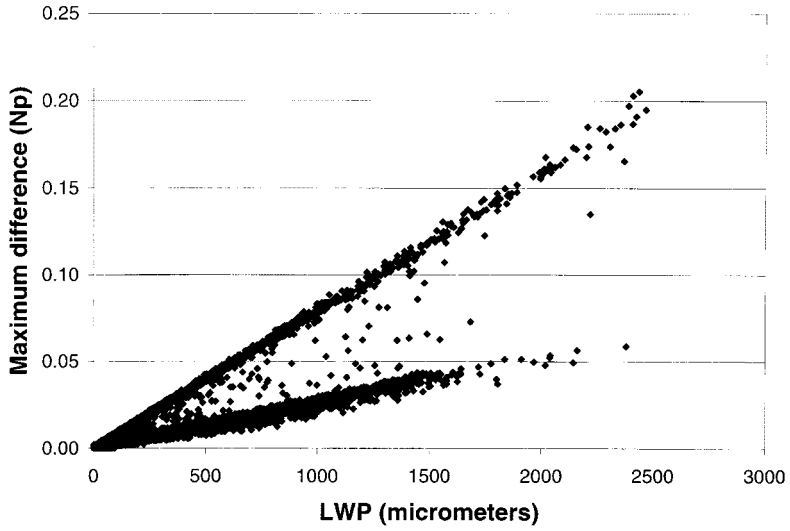

(c)

Fig. 5. Maximum differences between Mie solution opacities over five DSD models: (a) 22 GHz, (b) 32 GHz, and (c) 85 GHz.

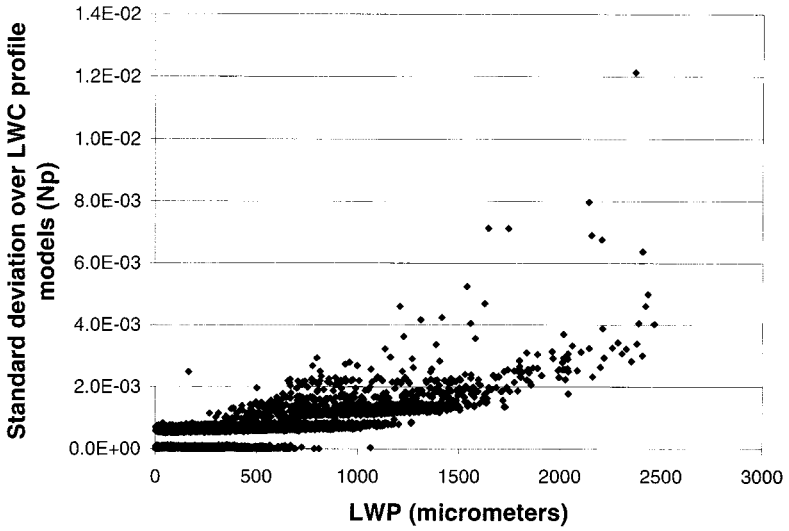

(a)

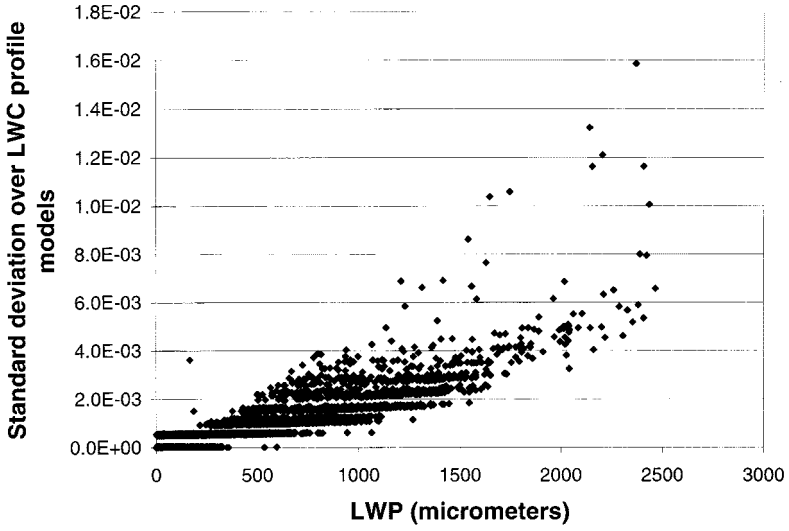

(b)

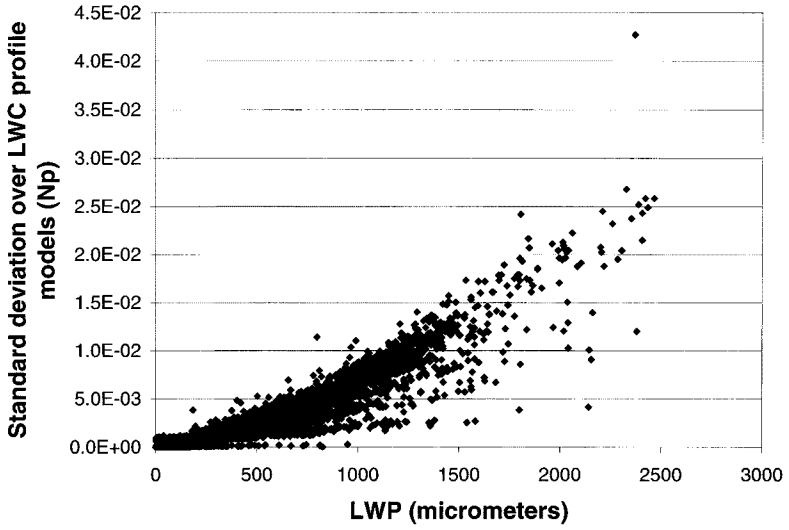

(c)

Fig. 6. Standard deviation of Mie solution opacities over three LWC profile models: (a) 22 GHz, (b) 32 GHz, and (c) 85 GHz.

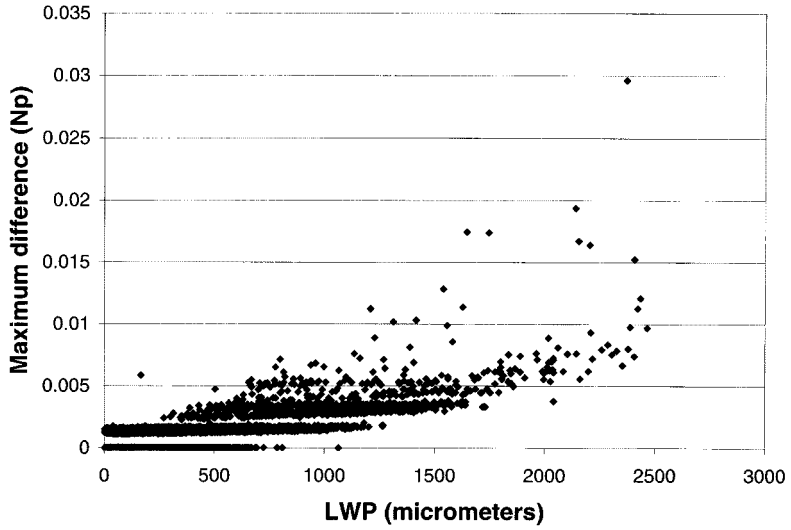

(a)

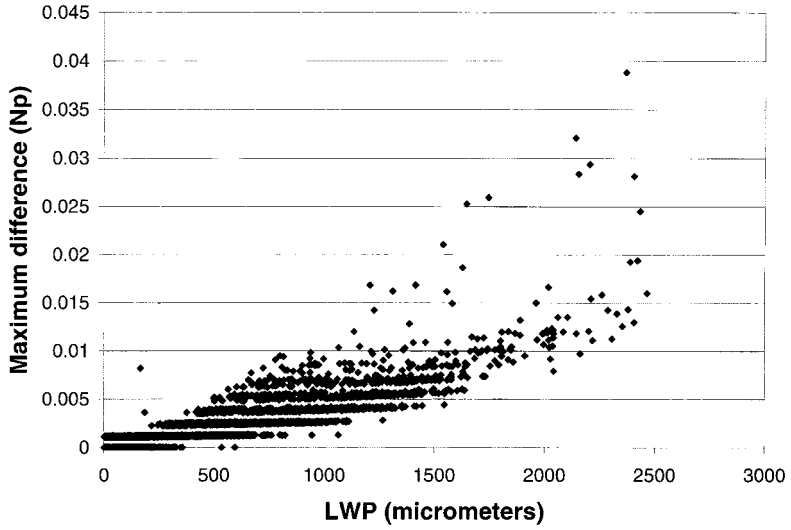

(b)

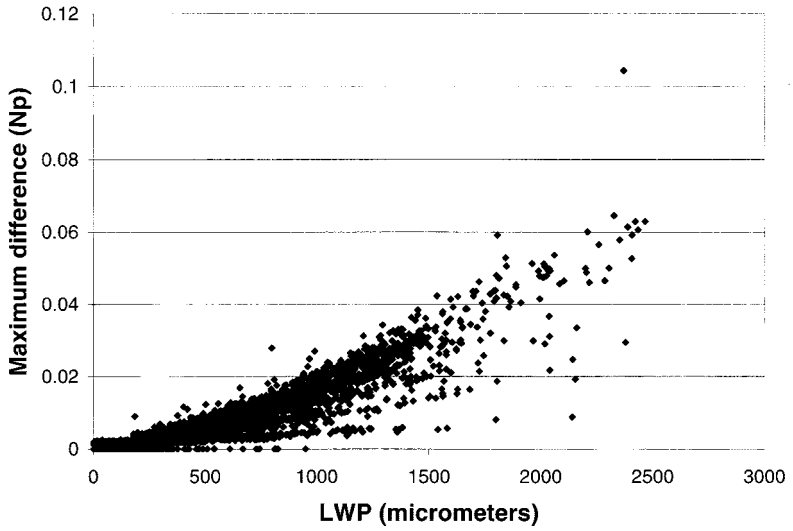

(c)

Fig. 7. Maximum differences between Mie solution opacities over three LWC profile models: (a) 22 GHz, (b) 32 GHz, and (c) 85 GHz.

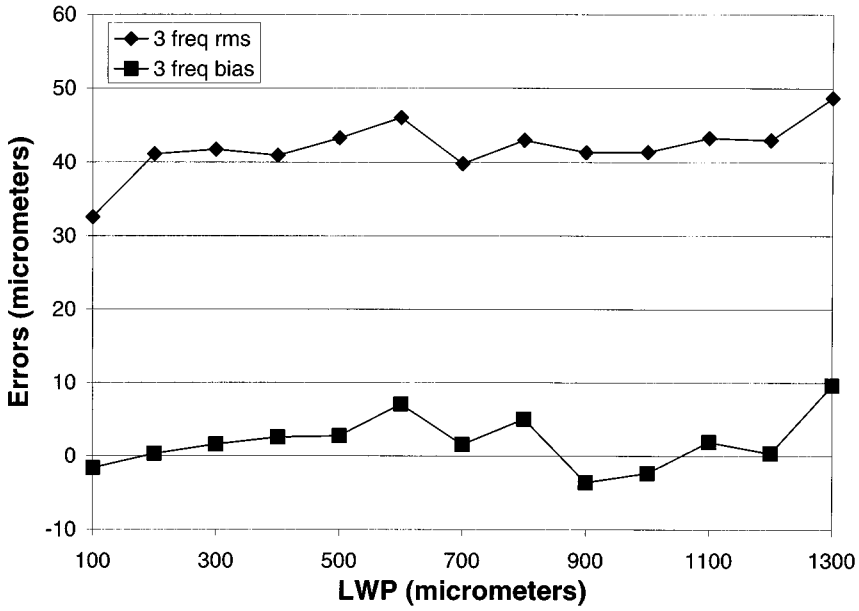

Fig. 8. Rms and bias errors as a function of liquid-water path for a three-frequency retrieval. The retrieval was trained with Rayleigh approximation opacities that had additional noise added to account for cloud-structure uncertainty.

These opacities were used to calculate retrieval coefficients. The new coefficients are

$$-95.9989 - 1651.09\tau_{22} - 259.203\tau_{32} + 1363.28\tau_{85} = \mathrm{LWP}_1. \tag{5}$$

A residual correction is also applied, given by

$$0 < \mathrm{LWP}_1 \leq 100\,\mu\mathrm{m}; \quad \mathrm{LWP}_2 = \mathrm{LWP}_1 - 6$$
$$100 < \mathrm{LWP}_1; \quad \mathrm{LWP}_2 = 1.037\mathrm{LWP}_1 - 16. \tag{5a}$$

When tested on Mie opacities calculated from the same model combinations as in Section III, the rms error is 43 μm, and the bias is -6 μm. The errors are shown in Fig. 8 as a function of LWP.

The error levels arising from the algorithm are insignificantly different from the errors arising from the algorithm in Section III, which assumed perfect knowledge of cloud DSD and LWC profile, and which was trained with Mie solution opacities. Thus, it is usually not necessary to be concerned with the cloud-modeling issues raised in this paper when frequencies are limited to 85 GHz or lower. However, the great majority of clouds in this database have small values of LWP (see Fig. 1). This can hide effects that arise only in the thicker clouds. The next section examines these thicker clouds.

VII. Thicker Clouds

As alluded to in an earlier section, the situation in which extremely thick clouds occur will now be discussed. The results shown in Fig. 3 indicate that the simulated 85-GHz opacities suffer a substantial departure from Rayleigh behavior for clouds containing at least 1000 μm LWP. In order to examine the potential effects this departure can have on liquid estimation, retrieval algorithms were developed using only clouds with LWP's of 1000 μm or more. These algorithms were tested on RaOb data that included only stratus clouds, as identified by the radiative-transfer code. The algorithms were tested on only this data because the stratus clouds showed the greatest departure from Rayleigh behavior and therefore, estimates of liquid in these clouds would be most affected by the presence or lack of knowledge regarding cloud structure.

The process for the first retrieval was like that in Section III. Full Mie solution opacities were used to train the algorithm, and then it was tested on full Mie solution opacities from RaOb's not in the training set. The resulting retrieval had an rms error level of 40 μm and a bias of -2 μm.

The second retrieval was trained with Rayleigh approximation opacities that included the extra noise term representing contributions from cloud-structure uncertainty. This was tested on the Mie RaOb's with greater than 1000 μm of LWP. This retrieval resulted in an rms level of 57 μm and a bias of -3 μm.

The rms error in the second case is almost 50% worse, illustrating the importance of DSD and LWC profile information in this case. These effects may also be evident in clouds with smaller LWP's. All of the clouds modeled for this work had unimodal distributions. Quite often, bimodal DSD's have been measured in clouds. For a fixed amount of liquid water, the bimodal distribution would have a greater number of droplets with larger radii, as the second peak of a bimodal distribution is usually at larger radii than the peaks in the distributions included in this work. These larger droplets would, of course, be more apt to show departure from Rayleigh behavior than the smaller droplets.

VIII. Conclusions

The potential improvement in cloud-liquid estimates that results from the inclusion of higher frequency information has been discussed before [9]. However, the difficulties that may arise due to the greater sensitivity of higher frequencies to cloud structure had not been previously addressed. This paper considers the effects that droplet-size distribution and liquid-water content profile have at the higher frequency.

TABLE II
PARAMETERS OF THE DROPLET-SIZE DISTRIBUTIONS TESTED

DSD model number	α	γ	Mode radius (micrometers)
1	2	1	5
2	2	1	10
3	2	1	15
4	2	1	Linearly increasing from 5 to 15 within cloud
5 – stratus	6	1	10
5 – fair weather cumulus	6	0.5	10

Reductions of 50% or more in the rms errors associated with liquid-water path estimates have been demonstrated. This improvement in error levels due to the addition of an 85-GHz channel is evident at all levels of liquid-water path. The improvement was shown based on atmospheric opacities calculated using the full Mie solution for droplet extinction. Typically, scattering effects have been ignored, even at 90 GHz. When atmospheric opacities at 85 GHz were examined, however, significant departures from Rayleigh-approximated behavior occurred for clouds with liquid-water paths of 1000 μm or greater.

The uncertainty in atmospheric opacity that arises from a lack of knowledge regarding the droplet-size distribution and the liquid-water content profile in observed clouds was examined. At 85 GHz, this uncertainty becomes significant for clouds as thin as 200 μm. A linear fit for this uncertainty as a function of liquid-water path was provided for 22, 32, and 85 GHz. This should be used as an additional error term, in addition to other noise sources, such as ΔT.

A retrieval algorithm was developed using opacities that were calculated by ignoring scattering effects and with this additional noise term. The errors in liquid-water estimates were shown to be small in general. However, for very thick clouds, these errors were more significant.

The results presented here show that at higher frequencies, in addition to questions about the validity of the Rayleigh approximation, one should be concerned about the modeling of clouds. In order to keep errors in retrieval algorithms as low as possible, it may be necessary to include information about the specific cloud types and droplet-size distributions that are expected.

APPENDIX
DROPLET-SIZE DISTRIBUTION AND LIQUID-WATER CONTENT PROFILE MODELS

For the simulations detailed in this paper, a unimodal, modified-gamma distribution has been used

$$p(r) = ar^{\alpha} \exp(-br^{\gamma}). \tag{A1}$$

In this equation, p is the number concentration of drops of radius r, and a and b can be calculated from the characteristic parameters α, γ and mode radius. This is a common DSD model equation [16], [19], and the shape parameters of the distribution are easily modified to represent various types of clouds.

Three different LWC profile models were used in this study. Two of them are based on adiabatic liquid-water content [17]. The third has a constant liquid-water density throughout the vertical extent of the cloud.

The five DSD models used are described in terms of their parameters in Table II. The first three models were included because a variety of droplet mode radii have been measured [21]. Also, in general, maritime clouds have a wider DSD than continental clouds [16]. The fourth model is included because measurements have indicated that the radius of droplets tends to increase with height within a cloud [36], [37]. For this model, the mode radius increases linearly from 5 to 15 μm from the base to the top of the cloud. The fifth model has DSD shape parameters and mode radii that vary from cloud to cloud, as in the widely used models of Deirmendjian [19]. In contrast to Diermendjian's results, Khrgian [36] found that a wide range of clouds could be modeled with the same shape parameters, which are the ones used for models 1–4.

For model 5, a simple algorithm for classifying clouds was created. This algorithm first checked for air-temperature inversions of at least 2K per vertical kilometer occurring within one kilometer of cloud top. If a suitable inversion was found, the cloud was classified as stratus. If no inversion was found, and if the vertical cloud extent was less than 2 km, the cloud was classified as fair-weather cumulus. If there was no inversion, and the vertical extent was greater than 2 km, the cloud was classified as cumulus congestus. Unfortunately, there was a problem calculating the DSD parameters for the cumulus congestus clouds, and RaOb soundings containing cumulus congestus clouds had to be discarded.

The three LWC profile models that were used are now described. The first is that in [41], which models LWC as

$$Q_{cld} = Q_{ad} * 0.6 * \exp\left(\frac{P - P_{lcl}}{60.0}\right) + 0.2 \tag{A2}$$

where Q_{cld} is the liquid in the cloud at the height with air pressure P (millibar), Q_{ad} is the predicted adiabatic liquid at that height, and P_{lcl} is the air pressure at cloud base. This model is a fit to an average of several measured profiles. The second model has an LWC profile that is a fixed fraction of the adiabatic LWC profile. This fraction is chosen such that the integrated liquid water is the same as that for the first model. The third model has a constant LWC throughout the vertical extent of the cloud, similar to that in [42]. The difference between this model and that of [41] is that here the constant is chosen such that the integrated liquid water is consistent with the first two models.

REFERENCES

[1] R. H. Dicke, R. Beringer, R. L. Kyhl, and A. B. Vane, "Atmospheric absorption measurements with a microwave radiometer," *Phys. Rev.*, vol. 70, no. 5 , pp. 340–348, Sept. 1946.
[2] D. H. Staelin, "Measurements and interpretation of the microwave spectrum of the terrestrial atmosphere near 1-centimeter wavelength," *J. Geophys. Res.*, vol. 71, pp. 2875–2881, June 1966.

[3] J. R. Wang, J. Zhan, and P. Racette, "Storm-associated microwave radiometric signatures in the frequency range of 90–220 GHz," *J. Atmos. Ocean. Technol.*, vol. 14, pp. 13–31, Feb. 1997.
[4] Y. Han and D. W. Thomson, "Multichannel microwave radiometric observations at Saipan during the 1990 tropical cyclone motion experiment," *J. Atmos. Ocean. Technol.*, vol. 11, pp. 110–121, Feb. 1994.
[5] G. M. Resch, "Inversion algorithms for water vapor radiometers operating at 20.7 and 31.4 GHz," Jet Propulsion Laboratory, Los Angeles, CA, TDA Prog. Rep. 42-76, Oct./Nov./Dec. 1983.
[6] E. R. Westwater and F. O. Guiraud, "Ground-based microwave radiometric retrieval of precipitable water vapor in the presence of clouds with high liquid content," *Radio Sci.*, vol. 15, pp. 947–957, Sept./Oct. 1980.
[7] E. R. Westwater, "The accuracy of water vapor and cloud liquid determination by dual-frequency ground-based microwave radiometry," *Radio Sci.*, vol. 13, pp. 677–685, July/Aug. 1978.
[8] B. L. Gary, S. J. Keihm, and M. A. Janssen, "Optimum strategies and performance for the remote sensing of path-delay using ground-based microwave radiometers," *IEEE Trans. Geosci. Remote Sensing*, vol. GE-23, pp. 479–484, July 1985.
[9] E. R. Westwater, "Ground-based microwave remote sensing of meteorological variables," in *Atmospheric Remote Sensing by Microwave Radiometry*, M. A. Janssen, Ed. New York: Wiley, 1993, pp. 145–213.
[10] F. Weng and N. C. Grody, "Retrieval of cloud liquid water using the special sensor microwave imager (SSM/I)," *J. Geophys. Res.*, vol. 99, pp. 25 535–25 551, Dec. 1994.
[11] J. R. Wang, T. T. Wilheit, and L. A. Chang, "Retrieval of total precipitable water using radiometric measurements near 92 and 183 GHz," *J. Appl. Meteorol.*, vol. 28, pp. 146–154, Feb. 1989.
[12] T. T. Wilheit, A. T. C. Chang, J. L. King, E. B. Rodgers, R. A. Nieman, B. M. Krupp, A. S. Milman, J. S. Stratigos, and H. Siddalingaiah, "Microwave radiometric observations near 19.35, 92 and 183 GHz of precipitation in tropical storm Cora," *J. Appl. Meteorol.*, vol. 21, pp. 1137–1145, Aug. 1982.
[13] J. Vivekanandan, L. Li, L. Tsang, and C. Chan, "Microwave radiometric technique to retrieve vapor, liquid and ice: Part II—Joint studies of radiometer and radar in winter clouds," *IEEE Trans. Geosci. Remote Sensing*, vol. 35, pp. 237–247, Mar. 1997.
[14] E. R. Westwater, J. B. Snider, and M. J. Falls, "Ground-based radiometric observations of atmospheric emission and attenuation at 20.6, 31.65, and 90.0 GHz: A comparison of measurements and theory," *IEEE Trans. Antennas Propagat.*, vol. 38, pp. 1569–1579, Oct. 1990.
[15] J. I. H. Askne and B. G. Skoog, "Atmospheric water—Vapor profiling by ground-based radiometry at 22 and 183 GHz," *Remote Sensing*, vol. GE-21, pp. 320–323, July 1983.
[16] H. R. Pruppacher and J. D. Klett, *Microphysics of Clouds and Precipitation*, 2nd ed. Dordrecht: Kluwer, 1997.
[17] X. Dong, "Microphysical and radiative properties of stratiform clouds deduced from ground-based measurements," Ph.D. dissertation, Penn State Univ., University Park, 1996.
[18] L. Li, J. Vivekanandan, C. H. Chan, and L. Tsang, "Microwave radiometric technique to retrieve vapor, liquid and ice: Part I—Development of a neural network-based inversion method," *IEEE Trans. Geosci. Remote Sensing*, vol. 35, pp. 224–235, Mar. 1997.
[19] D. Deirmendjian, *Electromagnetic Scattering on Spherical Polydispersions*. New York: American Elsevier, 1969.
[20] M. T. Chahine, "Interaction mechanisms within the atmosphere," in *Manual of Remote Sensing*, R. N. Colwell, Ed. Falls Church, VA: Amer. Soc. Photogramm., 1983, vol. I, pp. 165–230.
[21] E. E. Clothiaux, M. A. Miller, B. A. Albrecht, T. P. Ackerman, J. Verlinde, D. M. Babb, R. M. Peters, and W. J. Syrett, "An evaluation of a 94-GHz radar for remote sensing of cloud properties," *J. Atmos. Ocean. Technol.*, vol. 12, pp. 201–229, Apr. 1995.
[22] A. Slingo, R. Brown, and C. L. Wrench, "A field study of nocturnal stratocumulus—III: High resolution radiative and microphysical observations," *Q. J. Royal Meteorol. Soc.*, vol. 108, pp. 145–165, 1982.
[23] B. A. Albrecht, C. W. Fairall, D. W. Thomson, A. B. White, J. B. Snider, and W. H. Schubert, "Surface-based remote sensing of the observed and the adiabatic liquid water content of stratocumulus clouds," *Geophys. Res. Lett.*, vol. 17, pp. 89–92, Jan. 1990.
[24] G. L. Stephens and C. M. R. Platt, "Aircraft observations of the radiative and microphysical properties of stratocumulus and cumulus cloud fields," *J. Climate Appl. Meteorol.*, vol. 26, pp. 1243–1269, Sept. 1987.
[25] B. A. Albrecht, R. S. Penc, and W. H. Schubert, "An observational study of cloud-topped mixed layers," *J. Atmos. Sci.*, vol. 42, pp. 800–822, Apr. 1985.
[26] V. R. Noonkester, "Droplet spectra observed in marine stratus cloud layers," *J. Atmos. Sci.*, vol. 41, pp. 829–845, Mar. 1984.
[27] S. D. Slobin, "Microwave noise temperature and attenuation of clouds: Statistics of these effects at various sites in the United States, Alaska, and Hawaii," *Radio Sci.*, vol. 17, pp. 1443–1454, Nov./Dec. 1982.
[28] L. Tsang, J. A. Kong, E. Njoku, D. H. Staelin, and J. W. Waters, "Theory for microwave thermal emission from a layer of cloud or rain," *IEEE Trans. Antennas Propagat.*, vol. AP-25, pp. 650–657, Sept. 1977.
[29] E. N. Brown and R. R. Braham Jr., "Precipitation-particle measurements in trade-wind cumuli," *J. Meteorol.*, vol. 16, pp. 609–616, Dec. 1959.
[30] B. J. Mason, *The Physics of Clouds*. Oxford, U.K.: Clarendon, 1957.
[31] S. L. Cruz Pol, C. S. Ruf, and S. J. Keihm, "Improved 20- to 32-GHz atmospheric absorption model," *Radio Sci.*, vol. 33, no. 5, pp. 1319–1333, Sept./Oct. 1998.
[32] H. J. Liebe and G. A. HuffoManabe, "A model for the complex permittivity of water at frequencies below 1 THz," *Int. J. Inf. Millim. Waves*, vol. 12, pp. 659–675, June 1991.
[33] S. J. Keihm, M. A. Janssen, and C. S. Ruf, "TOPEX/Poseidon microwave radiometer (TMR)—III: Wet troposphere range correction algorithm and pre-launch error budget," *IEEE Trans. Geosci. Remote Sensing*, vol. 33, pp. 147–161, Jan. 1995.
[34] Y. Han, "Ground-based microwave radiometric remote sensing of the tropical atmosphere," Ph.D. dissertation, Penn State Univ. , University Park, 1992.
[35] G. W. Petty and K. B. Katsaros, "The response of the SSM/I to the marine environment—Part I: An analytic model for the atmospheric component of observed brightness temperatures," *J. Atmos. Ocean. Technol.*, vol. 9, pp. 746–761, Dec. 1992.
[36] S. Monson, *Cloud Physics*, A. K. Khrgian, Ed. Jerusalem, Israel, 1963.
[37] R. R. Rogers and M. K. Yau, *A Short Course in Cloud Physics*, 3rd ed. Oxford: Pergamon, 1989.
[38] J. B. Snider, H. M. Burdick, and D. C. Hogg, "Cloud liquid measurement with a ground-based microwave instrument," *Radio Sci.*, vol. 15, pp. 683–693, May/June 1980.
[39] M. K. Politovich, "Aircraft icing caused by large supercooled droplets," *J. Appl. Meteorol.*, vol. 28, pp. 856–868, Sept. 1989.
[40] F. T. Ulaby, R. K. Moore, and A. K. Fung, *Microwave Remote Sensing: Vol. 1, Microwave Remote Sensing Fundamentals and Radiometry*. Norwood, MA: Artech, 1981.
[41] C. J. Walcek and G. R. Taylor, "A theoretical method for computing vertical distributions of acidity and sulfate production within cumulus clouds," *J. Atmos. Sci.*, vol. 43, pp. 339–355, Feb. 1986.
[42] M. T. Decker, E. R. Westwater, and F. O. Guiraud, "Experimental evaluation of ground-based microwave radiometric sensing of atmospheric temperature and water vapor profiles," *J. Appl. Meteorol.*, vol. 17, pp. 1788–1795, Dec. 1978.

Justin P. Bobak (S'90–M'98) received the B.S., M.S., and Ph.D. degrees in electrical engineering, all from the Pennsylvania State University, University Park, in 1992, 1994, and 1998, respectively.

His M.S. research focused on characterizing the stability of noise sources used in microwave radiometry. During his Ph.D. studies, he modeled the atmospheric turbulence signature in water vapor radiometer data and compared various cloud models used at microwave frequencies. He is currently a Member of the Remote Sensing Physics Branch of the Naval Research Laboratory, Washington, DC. He is part of the design team for an airborne polarimetric radiometry instrument (APMIR) and is responsible for maintaining the absolute accuracy error budget for this instrument.

Christopher S. Ruf (S'85–M'87–SM'92) received the B.A. degree in physics from Reed College, Portland, OR, in 1982, and the Ph.D. degree in electrical and computer engineering from the University of Massachusetts, Amherst, in 1987.

He was with the Microwave Remote Sensing Laboratory, University of Massachusetts, Amherst, from 1983 to 1988. He then joined the technical staff at NASA's Jet Propulsion Laboratory (JPL), and in 1992, he left JPL to join the faculty of The Pennsylvania State University, University Park as an Associate Professor of Electrical Engineering. His current research activities include participation in the TOPEX/Poseidon, GEOSAT Follow-On, Jason-1, and NPOESS CMIS flight missions, ground-based atmospheric remote sensing using millimeter radars, radiometers, and synthetic aperture interferometric radiometry.

Dr. Ruf received the 1997 GRS-S Transactions Prize Paper Award and the 1999 IEEE Judith A. Resnik Award. He is a member of the AGU and Commission F of URSI. He is the current Editor and past Associate Editor of the *IEEE GRS-S Newsletter*. He is a past Guest Editor and Associate Editor for *Radio Science*. He serves or has served on the Technical Program Committees of IGARSS 1996, 1998, 1999, and 2000, and the μRad'96 Specialist Meeting on Microwave Radiometry.